



Mechanical and electrochemical behaviour of electron beam welded commercially pure aluminium using oscillating beam

Aakash Rathore¹ · Jeetendra Kumar Singh¹ · Gour Gopal Roy¹ · Indranil Manna¹ · Jyotsna Dutta Majumdar¹

Received: 15 January 2024 / Accepted: 3 August 2024 / Published online: 20 August 2024
© International Institute of Welding 2024

Abstract

The present study evaluates the effect of beam oscillation on the mechanical and electrochemical properties of electron beam welded commercially pure aluminium. The circular beam oscillation diameters of 1 mm and 2 mm have been used while keeping all the other welding parameters constant. The churning effect of beam oscillation led to the formation of a broader fusion zone compared to static beam joint. The fusion zone of a static beam weld consists of equiaxed and columnar structures, while the fusion zone of an oscillated beam weld mainly consists of equiaxed structures. The joints produced using beam oscillation have less porosity (0.01%) than static beam joint (0.02%). Also, the pores were more evenly distributed in the oscillated beam joints. The application of circular beam oscillation of diameters 1 mm and 2 mm increased the microhardness (56 VHN and 58 VHN) as compared to the static beam joint (52 VHN) and base metal (45 VHN). The tensile strength of aluminium (102 MPa) decreased slightly after electron beam welding (99 to 91 MPa). Beam oscillation reduced the tensile strength further (91 MPa and 93 MPa) as compared to the static beam joint (99 MPa), whereas the percentage elongation increased (9 to 17%) due to beam oscillation. Beam oscillation has reduced the corrosion rate from 0.02 mm/year (base metal) to 0.001 mm/year (oscillated beam weld). The mechanism of variation in mechanical and electrochemical properties of electron beam welded aluminium with the application of beam oscillation has been established.

Keywords Aluminium · Electron Beam Welding · Beam oscillation · Microstructure

1 Introduction

Aluminium alloys have been extensively used in different industrial applications such as aerospace, automobiles, pressure vessels and railways because of their high specific strength and excellent thermal conductivity [1, 2]. Now, the focus is to attain a high-quality weld joint. Aluminium alloy welding has been challenging yet quite active. For years, industries have routinely used arc welding to join aluminium alloys. However, the low welding speed and high heat input of conventional arc welding cause significant deformation, leading to the formation of cracks and porosities [2, 3]. The main difficulty of welding aluminium alloys is the formation

of an oxide layer on the surface. Fusion welding methods like tungsten inert gas (TIG) welding are mainly used for aluminium welding, which often encounters defects like porosities and microcracks [1, 4]. Aluminium welding by solid-state welding methods generally has defects like oxide layer formation, surface porosity and lack of penetration. Additionally, aluminium alloys like Al6061 or Al5154 contain trace amounts of magnesium, which conventional arc welding methods cannot appropriately weld. The cracks generally initiate at the interface of base metal and heat-affected zone (HAZ), which propagates further in the fusion zone (FZ), resulting in inferior mechanical properties [5]. These problems can be easily solved by employing high-energy beams like laser and electron beams for welding aluminium and its alloys. The ability of laser beam welding to perform deep welds has been reported to enhance weld quality and decrease the material's susceptibility to defect formation. However, porosity formation in laser welded aluminium alloy affects its tensile strength and fatigue resistance. In addition, the high reflectivity of aluminium alloys reduces the laser energy absorption, which potentially affects the

Recommended for publication by Commission IV - Power Beam Processes.

✉ Jyotsna Dutta Majumdar
jyotsna@metal.iitkgp.ac.in

¹ Metallurgical and Materials Engineering Department, IIT Kharagpur, Kharagpur, India

weld quality [6–8]. Vänskä et al. [9] showed the effect of beam oscillation (BO) in laser welding of 5-mm-thick stainless-steel tubes. They used an oscillated beam to remove the small gaps and misalignment in the welding, though tiny pores were found afterwards. Wang et al. [10] studied the effect of BO frequency in the suppression of porosity in AA6082 aluminium alloy joints prepared using laser-MIG hybrid welding. The porosity percentage was significantly reduced by increasing the beam oscillation frequency. The reduction in the porosity was attributed to the improved keyhole stability at higher oscillation frequencies. Meng et al. [11] used high-frequency laser beam oscillation and synchronous wire-powder feeding to overcome the problem of evaporation and burning loss of alloying elements in joining AA2219 aluminium alloy. The high-frequency laser beam oscillation coupled with synchronous wire-powder feeding was found to reduce the porosity of the weld joint from 10.7 to 0.7% and improve the tensile strength by 12% as compared to the unoscillated beam. They attributed the reduction in porosity to the stirring effect of a high-frequency oscillating beam, which breaks and inhibits the growth of dendrites. Wang et al. [12] studied the effect of beam oscillating patterns on weld characterisation of laser welding of AA6061-T6 aluminium alloy. They studied the three different oscillating patterns and showed that the circular BO promoted the formation of equiaxed grains in the FZ. Berend et al. [13] studied the effect of high-frequency BO for keyhole stability in aluminium alloy laser beam welding. They showed that the stable keyhole reduced the humping effects of the weld zone.

Electron beam (EB) welding is another high-energy density welding process. EB welding produces the fusion by concentrated electron beams impinging upon the workpiece. During the irradiation with an electron beam, the electron's kinetic energy is transferred to atoms, generating intense heat leading to the melting and welding of materials. The EB welding may be conducted in two modes: conduction and keyhole. The keyhole welding mode is preferred for joining thicker sections [8, 14]. EB welding uses focused electron beams, which reduces the size of the HAZ as compared to conventional welding processes. Other advantages of EB welding, such as low heat input, deep penetration, repeatability and minor distortion, make it superior to traditional welding methods [15]. EB welding has successfully been applied for the welding of materials like aluminium (Al), stainless steel (SS), titanium (Ti) and its alloys, zirconium (Zr) and niobium (Ni) [16, 17]. The main process parameters for EB welding are acceleration voltage, beam current, weld speed and beam oscillation. Among these parameters, BO is an important parameter that has been reported to stabilise the keyhole and reduce porosity. In addition, BO has also been reported to make the weld smoother without any spatter [16]. Gabreili et al. [17] used EB welding to join

AA6061 T651 alloys to develop distortion-free welding with increased penetration depth and controlled residual stress. Zuhair et al. [18] studied the effect of EB welding parameters on the tensile strength of AA1350 alloys and reported a reduction in the impact toughness of the joint because of the recrystallisation processes due to the localised heating produced by the electron beam. Moschinger et al. [19] studied the influence of beam current on the porosity formation of the EB welded aluminium alloy (AW6082). They showed that the beam current influences the porosity but could not establish a direct relationship between them. Zhan et al. [20] conducted a comparative study of the laser beam and EB welding of 5A06 aluminium alloy. They showed that the weld bead cross-section area of laser beam welding is 4.34 mm², while that for EB welding is 2.6 mm². They also showed that the grain size of laser beam welds was more significant than the EB welded grains size. Finally, they concluded that the weld quality of EB welded joints was superior to that of laser welded joints and that laser could not replace EB welding. Kar et al. [21] studied the effect of process parameters on the formation and distribution of porosities in EB welded dissimilar joints of AA6061 and AA2024 aluminium alloys. They showed that the BO and higher scan speed produce smooth welds with less spatter. Jeetendra et al. [22] showed that the yield strength (YS) and ultimate tensile strength (UTS) of the EB welded commercially pure titanium (Cp-Ti) joint remained unchanged while the microhardness was increased as compared to the base metal.

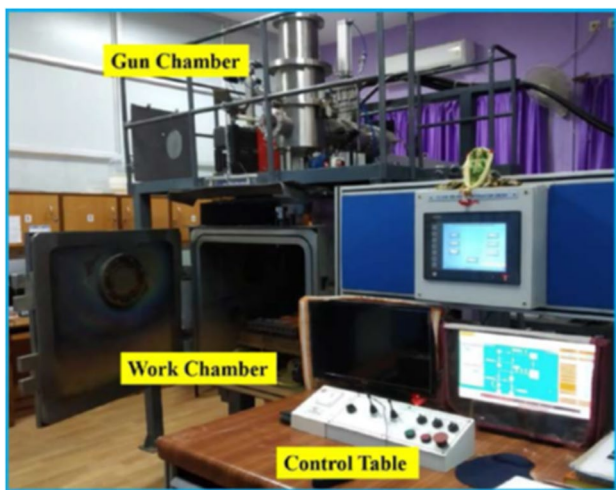
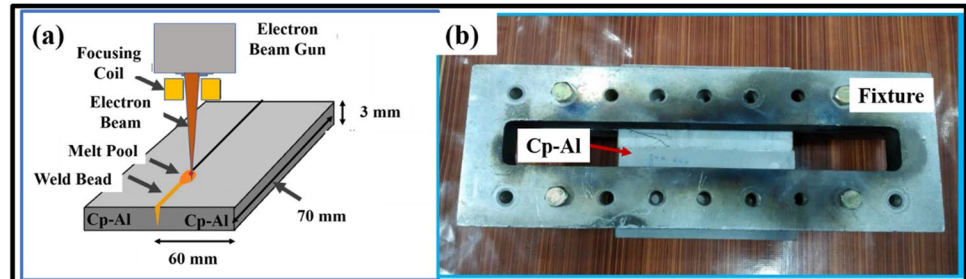
Though the influence of EB welding parameters such as beam current, welding speed and oscillation frequency on the similar joining of aluminium and its alloys has been studied in detail, however, the effect of variation in oscillation diameter on the microstructure, porosity distribution and mechanical and electrochemical properties has yet to be studied in detail. In the present work, EB welding of commercially pure aluminium (Cp-Al) similar joints has been performed at an optimum acceleration voltage, beam current (corresponding to the formation of defect-free weld zone) and varied BO diameter. A thorough microstructural examination was performed to understand the effect of circular BO on the microstructures and its effect on the mechanical and electrochemical properties of the joints.

2 Experimental procedures

In the present study, Cp-Al was used as base metal. The chemical composition of as-received Cp-Al obtained from X-ray fluorescence spectroscopy (XRF) and its mechanical properties (obtained from mechanical testing) are given in Table 1. The plates with dimensions of 70×60×3 mm³ (length×breadth×height) were taken from cold rolled

Table 1 Chemical composition and mechanical properties of as-received Cp-Al

Chemical compositions	Elements	Si	Fe	Ti	Mn	Zn	Al
	Content (wt%)	0.15	0.25	0.05	0.05	0.05	99.45
Mechanical properties	Ultimate Tensile Strength —102 MPa		Ductility —23%				
	Yield strength —65 MPa						

Fig. 1 a Schematic diagram of EB welding of Cp-Al, b Cp-Al plates fitted in the fixture in butt welding configuration**Fig. 2** Electron beam welding setup at IIT Kharagpur

sheets. The length side (70 mm) was used for the butt welding of Cp-Al, which is transverse to the rolling direction. The cross-sections of the prepared coupons were mechanically polished to a roughness of $5\ \mu\text{m}$ (average surface roughness) using emery paper before welding. Figure 1a shows the schematic diagram of EB welding of Cp-Al. The clamps tightly fitted the two adjoining plates to ensure a negligible air gap between them, as shown in Fig. 1b.

2.1 Selection of process parameters

Welding was performed using an 80-kV and 12-kW EB welding machine at IIT Kharagpur (Make: Bhabha Atomic Research Centre (BARC); Department of Atomic Energy (DAE)) (as shown in Fig. 2). The EB welding parameters were set at an accelerating voltage of 55 kV, beam current of

36 mA, weld speed of 750 mm/min and oscillation frequency of 500 Hz. The circular beam oscillation of two oscillation diameters, 1 mm and 2 mm, were used. In the study, circular beam oscillation was used as the EB welding machine at IIT Kharagpur only has a circular beam oscillation configuration. The optimum parameters for the study were selected after a series of bead-on-plate welding experiments on the same Cp-Al coupons. The parameters resulting in full-depth penetration with no visual defects have been chosen for the EB welding. Selected parameters are listed in Table 2.

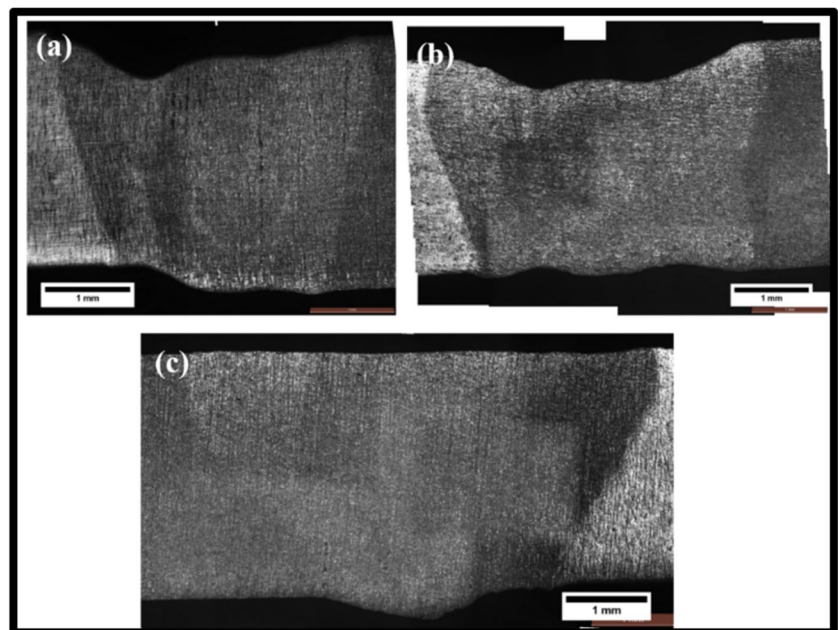
A 3D non-contact optical surface profilometer (Model: Contour GT, make: Bruker) was utilised to calculate the average surface roughness of as-received and FZ of EB welded Cp-Al samples. For three-dimensional (3D) analysis of porosities, the X-ray computed tomography (XCT) technique was employed using a GE Phoenix® model: V/TOME/XS. For microstructural observation, samples were cut perpendicular to the weld direction using an abrasive cutter. Subsequently, specimens were polished using different grades of SiC emery papers ranging from 240 to 2000 grit size. Keller's reagent (1.5 ml of hydrochloric acid, 2.5 ml of nitric acid, 1 ml of hydrofluoric acid and 95 ml of distilled water) was used as an etchant to reveal the microstructure. The weld joints were then observed under an optical microscope (Model: DM6000 M, Make: Laica®). A scanning electron microscope (Model: Merlin SEM, GEMINI 2, Make: ZEISS®) was used for the higher magnification images. ImageJ software was used to measure the average dendritic lengths. The phases present in the microstructure were analysed using an X-ray diffractometer (Model: D8 Advance diffractometer, Make: Bruker, Germany), at an operating voltage of 40 kV and current of 40 mA with Cu $K\alpha$ radiation. The phase identification was performed using TOPAS software. Microhardness measurements of both the weld zone and the as-received Cp-Al were obtained with the

Table 2 EB welding parameters used in the present study

Butt joints	Accelerating voltage (kV)	Beam current (mA)	Scan speed (mm/min)	Oscillation frequency (Hz)	Oscillation diameter (mm)
Joint 1	55	36	750	0	0
Joint 2				500	1
Joint 3				500	2
Oscillation type —Circular oscillation			Work chamber pressure — 5×10^{-5} mbar		
Working distance —432 mm			Number of pass —01		
Gun chamber pressure — 5×10^{-6} mbar					

help of a Vickers microhardness testing machine (Model: VMHT-001, Make: UHL®) at 10 gf applied load and an indentation time of 10 s. The gap in the two adjacent indentation points was 0.25 mm, and the microhardness values were measured across the cross-section, which was 1 mm below the top surface of the joined samples. The tensile testing was performed using an Instron machine (Model: INSTRON 3365) at a cross-head speed (displacement rate) of 0.5 mm/min with a maximum load of 5 kN and a gripping distance of 25 mm. The fractography of the fractured samples of tensile testing was observed under a scanning electron microscope (SEM). Finally, corrosion analysis of as-received and EB welded Cp-Al samples was done by potentiodynamic polarisation testing using a three-electrode system (Model: Metrohm Autolab, Netherlands). An Ag/AgCl electrode was used as the working electrode, while platinum was used as the counter electrode. The exposed area was kept constant (1 cm²) for all the tested samples. Polarisation test was performed at a scanning rate of 0.2 mV/s, from −0.5 V (Ag/AgCl) to +1.0 V (Ag/AgCl).

Fig. 3 Optical macrographs of the cross-section of EB welded Cp-Al joints prepared using a static beam and oscillated beam having oscillation diameter of **b** 1 mm and **c** 2 mm



3 Results and discussion

3.1 Fusion zone geometry

Figure 3 shows the optical macrographs of the weld zone of EB welded Cp-Al joints prepared using (a) static beam and oscillated beam having oscillation diameter of (b) 1 mm and (c) 2 mm. From Fig. 3a, it may be noted that welding without BO has the formation of an undercut. The introduction of BO reduces the undercut and the undercut is negligible for the joint prepared with oscillation diameter of 2 mm. The undercut for joint 1 is 0.41 mm; for joint 2 is 0.30 mm; for joint 3, it is negligible. This reduction in the undercut of the joint developed by beam oscillation may be attributed to the lower heat input per unit length and rapid quenching of the weld zone. Figure 4a and b shows no spatter was present in EB welded Cp-Al joints using a static or oscillated beam. In this regard, it should be mentioned that a similar observation of the formation

Fig. 4 Top surface images of EB welded Cp-Al joints prepared using **a** static beam and **b** oscillated beam (1 mm diameter)

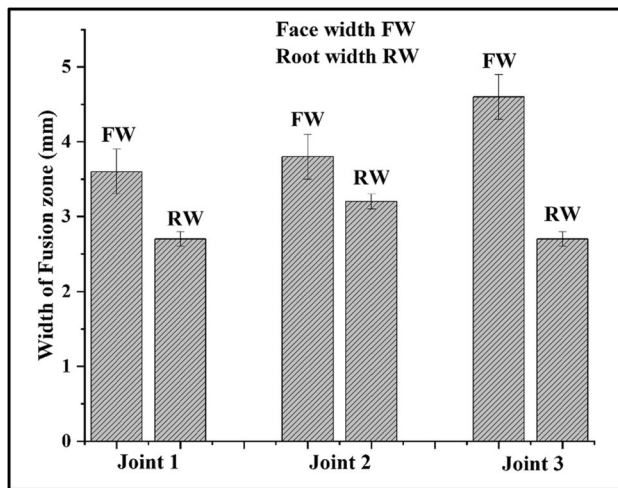
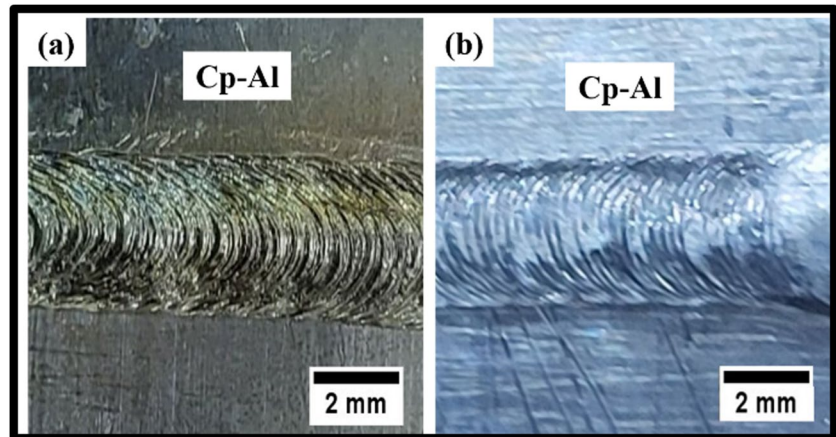


Fig. 5 Fusion zone width on the face and root side of the EB welded Cp-Al joints

of smooth surfaces without any spatter was earlier reported by several authors [12, 23, 24]. Figure 5 shows the FZ width, measured at the face and root side of the weld. The FZ shape is triangular, with the face having the highest width and the root having the lowest width. The face width and root width are higher for oscillated beam welds than static beam welds, and the difference between face and root is highest when the oscillation diameter is 2 mm.

3.2 Surface roughness

Figure 6 shows the 3-dimensional surface topography of (a) as-received Cp-Al, and EB welded Cp-Al joints prepared using (b) static beam, and oscillated beam having oscillation diameter of (c) 1 mm and (d) 2 mm. Figure 7 summarises the average surface roughness measured on the top surface of the as-received and EB welded Cp-Al joints. The surface roughness of the welded samples was measured in the FZ (as marked in Fig. 6). From Fig. 6 and Fig. 7, it may be noted

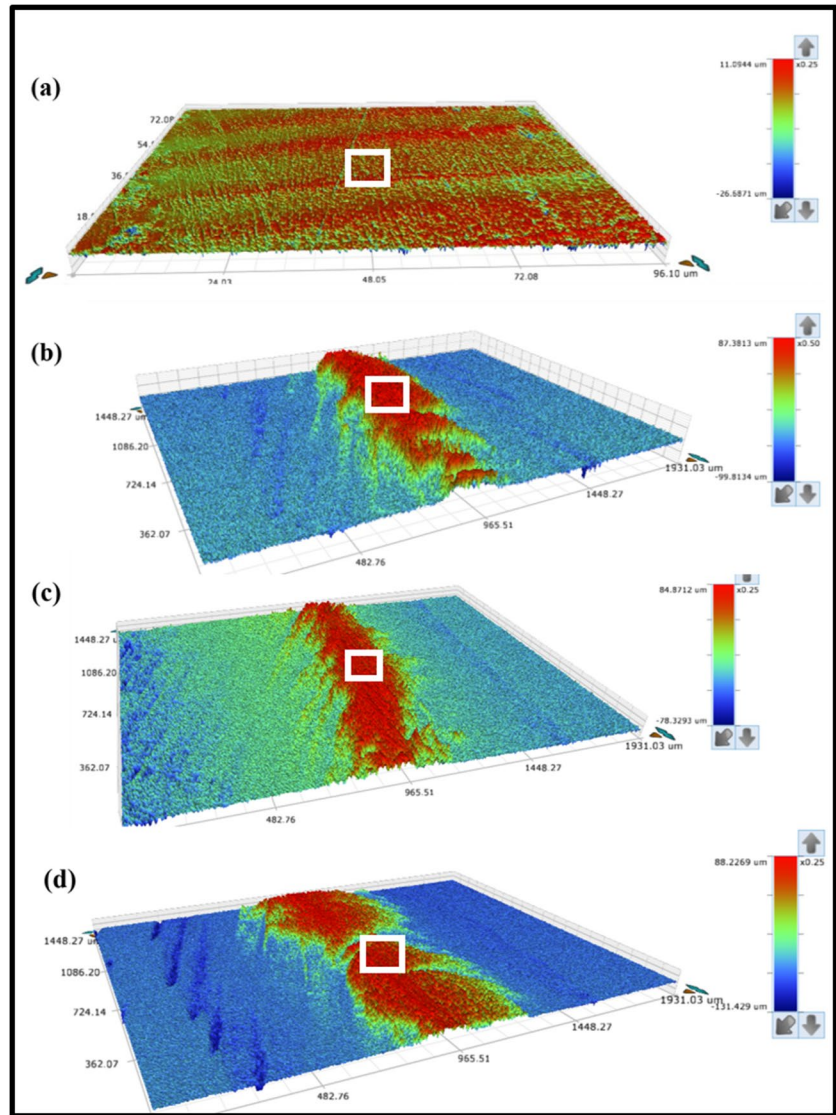
that due to EB welding, there is an increase in the average surface roughness from 1.05 μm of as-received Cp-Al to 17–21 μm for EB welded Cp-Al under the present set of parameters. This increase in the average surface roughness due to EB welding may be attributed to the surface tension-driven flow of material on the surface. Increased surface roughness was observed in oscillated beam welds, which may be attributed to the intense churning of the circular oscillated beam.

3.3 X-ray tomography

Figure 8a and b shows the 3D X-ray tomography images of the pores present in EB welded Cp-Al joints prepared using (a) static beam (joint 1) and (b) oscillated beam of oscillation diameter 2 mm (joint 3). From Fig. 8a, it may be observed that the distribution of porosities in joint 1 prepared using a static beam is very uneven and mostly concentrated at the interface of base metal and FZ. In joint 3, prepared using an oscillated beam, the pores are more evenly distributed across the weld zone, which may be attributed to better mixing produced due to the intense churning action of the oscillated beam. The weld joint prepared using static beam shows an increased porosity percentage in the weld zone (0.02%) as compared to the joint prepared with BO (0.01%). From Fig. 8a and b, it may be observed that all the joints have the presence of porosities. By observing the weld bead, joint 3 has a well-defined shape without undercutting or crack formation. Hence, it may be concluded that minimising porosities requires optimum oscillation diameter.

Figure 8c and d illustrates the pores' sphericity of EB welded Cp-Al as a function of pore diameter. The pores formed in a joint prepared using a static beam are less spherical in shape (Fig. 8c) and their size varies from 50 to 390 μm . The introduction of BO of diameter 2 mm makes the pores more spherical (Fig. 8d), though their size remains almost identical (50 to 380 μm). Porosities in the EB welding are due to the entrapment of the dissolved gases caused

Fig. 6 3D constructed roughness diagrams of **a** as-received Cp-Al and EB welded Cp-Al joints prepared using **b** static beam and oscillated beam having oscillation diameter of **c** 1 mm and **d** 2 mm



by rapid solidification. Dinda et al. [25] studied the effect of BO in EB welded DP600 steel to Al 5754 alloy. They showed that BO with optimum oscillation diameter improves the weld quality by reducing the amount and size of porosity as compared to static beam.

3.4 Microstructural studies

Figure 9 shows the microstructure of the FZ and base metal interface of EB welded Cp-Al joints. The transverse cross-sectional microstructure of the weld zone consists of columnar dendrites. The presence of dendritic structure may be due to the variable cooling rate during weld pool solidification. Microscopic analysis revealed that columnar dendrites usually comprised of more than 80% of the entire weld zone, while the area fraction of equiaxed grains was lower. The epitaxial solidification was the main

reason for columnar dendrite's growth near the fusion line. Epitaxial solidification generally advances in a path parallel to the largest thermal gradient towards the weld centre. The growth rate reaches its highest value at the weld centre after starting from zero at the fusion line [26]. Figure 9a has columnar dendrites of an average length of 87 μm , while the average lengths of dendrites were lower for welds prepared with oscillating beams (Fig. 9b and Fig. 9c). The average dendritic length in the oscillating beam weld of diameter 1 mm is 72 μm and for diameter 2 mm is 68 μm . This reduction in the dendritic length due to beam oscillation may be attributed to the tearing effect produced by the intense churning action of BO. A narrow HAZ may be observed near the fusion line of all three welds, as shown in Fig. 9a–c. The HAZ width was not affected by the introduction of beam oscillation or change in oscillation diameter.

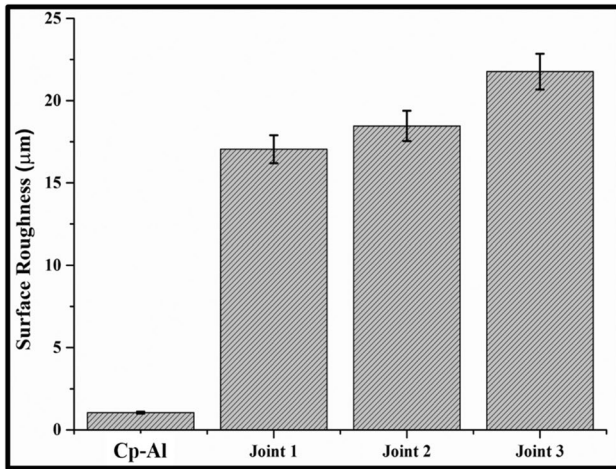


Fig. 7 Bar charts showing the variation of average surface roughness of as-received Cp-Al, and the EB welded Cp-Al joints prepared with static beam (joint 1), and oscillated beam having the oscillation diameter of 1 mm (joint 2) and 2 mm (joint 3)

Figure 10 shows the cross-section of FZ of the EB welded Cp-Al joints. From Fig. 10, it may be observed that the microstructure formed in the FZ is generally of equiaxed form. The BO hinder the dendrite’s growth and promotes the formation of equiaxed grains. The amount of equiaxed structure increases from joint 1 to joint 3 which may be attributed to the effect of BO. Figure 11 shows the effect of circular beam oscillation on the heat flow, which promotes the formation of equiaxed grains and reduces the formation of columnar dendrites. From Fig. 11a, it is clear that the molten pool without beam oscillation has a lower cooling rate than the oscillated beam weld due to the axial flow of the static beam weld. From Fig. 11b, it may be observed that the circular melt flow in oscillated beam welds stirs the molten pool continuously. The stirring of the weld pool generates many small turbulences among the dendrites, which increases the rate of the re-melting and breaking of dendrites. The circular melt flow drives the broken and partially melted grains into the molten pool, providing more nuclei for equiaxed grain growth. Therefore, the oscillated beam weld has more equiaxed grains. Since the equiaxed grains are isotropic, with an

Fig. 8 3D micro CT image of porosity distribution of EB welded Cp-Al joints prepared using **a** static beam, **b** oscillated beam (2 mm); weld sphericity vs pore diameter using **c** static beam and **d** oscillated beam (2 mm)

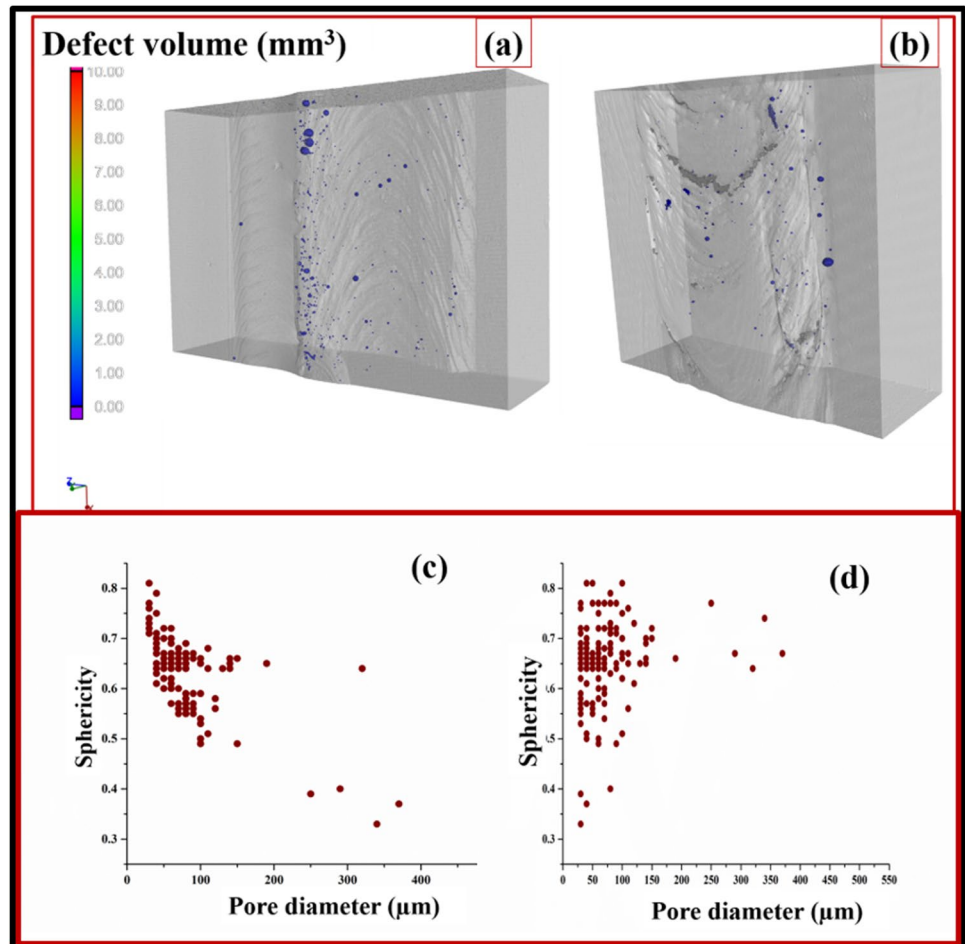


Fig. 9 Optical micrographs of the FZ and base metal interface of EB welded Cp-Al joints prepared using **a** static beam, oscillated beam having oscillation diameter of **b** 1 mm and **c** 2 mm

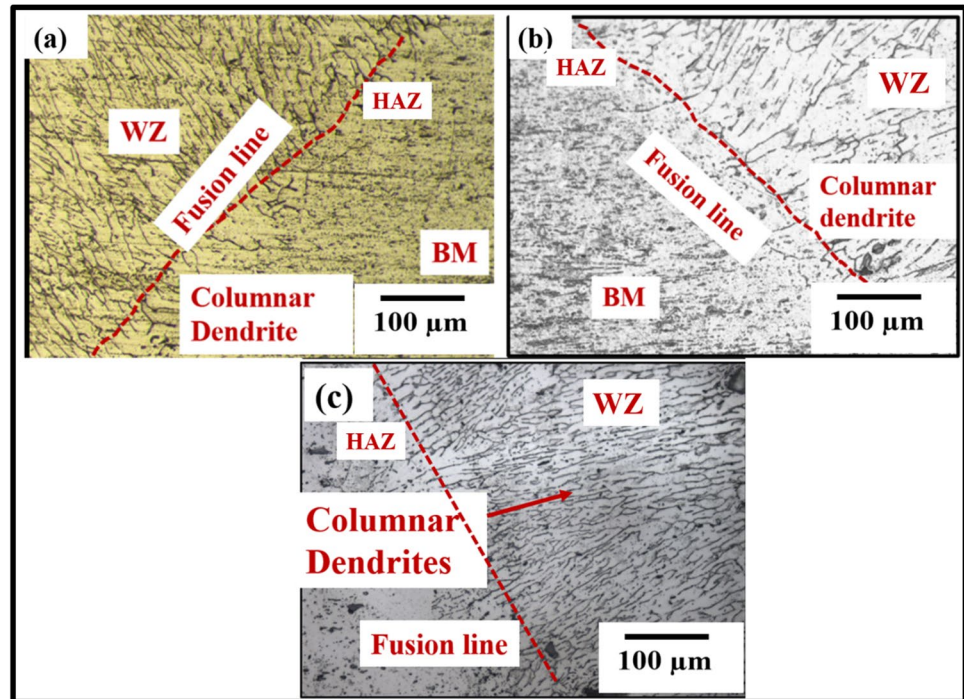
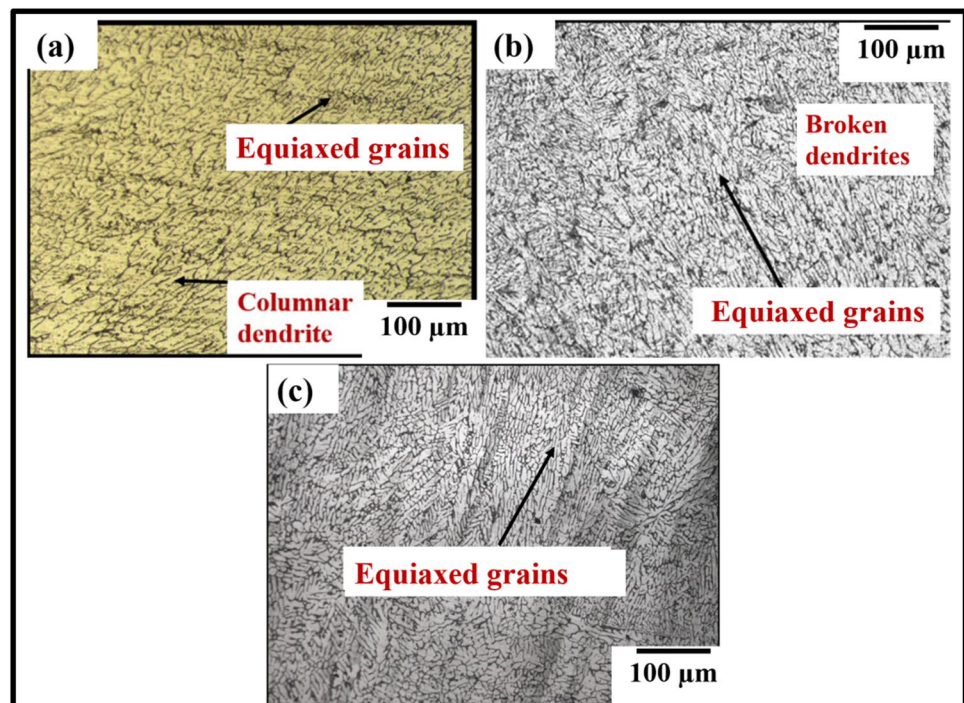


Fig. 10 Optical micrographs of the FZ of EB welded Cp-Al joints prepared using **a** static beam and oscillated beam having oscillation diameter of **b** 1 mm and **c** 2 mm



increase in equiaxed structure, the strain is also improved, thus improving the ductility of the weld joints [12, 27].

Figure 12 shows the high magnification scanning electron micrographs of the transverse cross-section of the FZ of the EB welded Cp-Al joints prepared with (a) static beam and oscillated beam having oscillation diameter of (b) 1 mm and (c) 2 mm. The cross-section microstructure of FZ prepared

without BO is a mixture of equiaxed and columnar dendritic structures. The average grain size in the FZ of the joint prepared using a static beam is the highest (15 μm) as compared to 12 μm and 10 μm for the joints prepared using 1 mm and 2 mm beam oscillation diameters, respectively. Joint 2, prepared with an oscillation diameter of 1 mm, shows the presence of both columnar dendrites and equiaxed grains.

Fig. 11 Schematic drawings showing the effect of melt flow on microstructure formation, **a** static beam and **b** oscillated beam

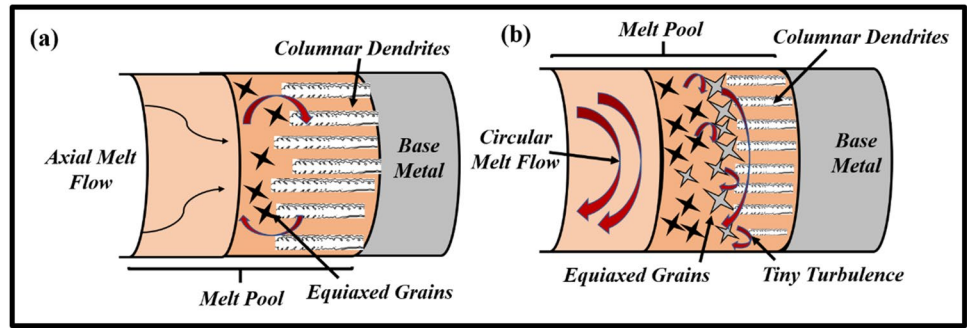
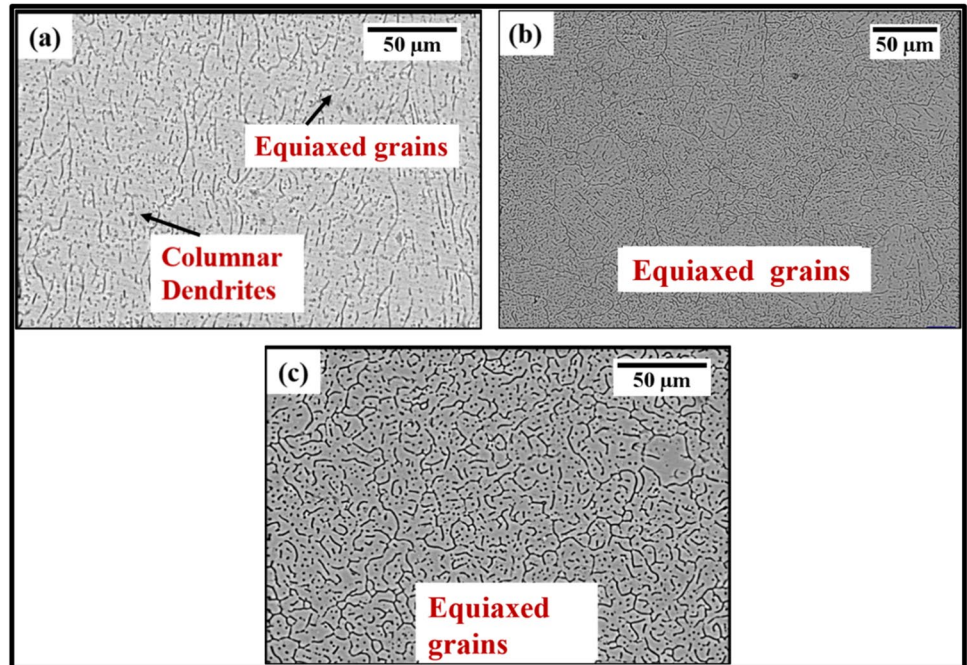


Fig. 12 Scanning electron micrographs of the FZ of EB welded Cp-Al joints prepared using **a** static beam (joint 1) and oscillated beam having oscillation diameter of **b** 1 mm (joint 2) and **c** 2 mm (joint 3)



The joint prepared with a 2-mm oscillation diameter shows a maximum amount of equiaxed grains as compared to joint 1 and joint 2. From Fig. 12, it is clear that the optimum oscillation diameter leads to grain refinement and also increases the amount of equiaxed grains in the FZ.

3.5 Phase analysis

Figure 13 displays the X-ray diffraction spectra obtained from the as-received and EB welded Cp-Al samples. The spectra demonstrate the presence of only α -phase in the weld zone. Lattice strain is also calculated by analysing XRD spectra using Scherrer’s formula. From Fig. 14, it may be observed that the magnitude of lattice strain introduced in the joint prepared with the static beam is lower than the as-received Cp-Al. Beam oscillation tends to increase the lattice strain, and it is maximum for joint 3 prepared with a 2-mm oscillation diameter, though it is still lower than the as-received Cp-Al. The increase in the lattice strain with

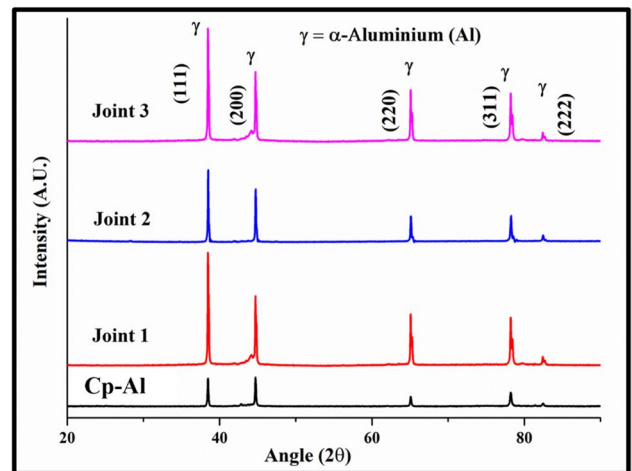


Fig. 13 X-ray diffraction profiles of the as-received and EB welded Cp-Al joints prepared using static beam (joint 1) and oscillated beam having oscillation diameter of 1 mm (joint 2) and 2 mm (joint 3)

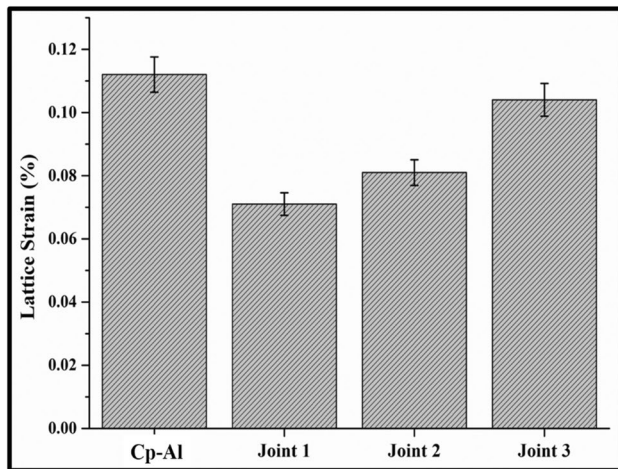


Fig. 14 Bar diagram of lattice strain of Cp-Al and EB welded Cp-Al joints prepared using static beam (joint 1) and oscillated beam having oscillation diameters of 1 mm (joint 2) and 2 mm (Joint 3)

an increase in oscillation diameter may be attributed to the effective lower heat input per unit length, which led to the faster cooling rate in oscillated beam joints. A similar observation was also reported by Jeetendra et al. [28].

3.6 Microhardness measurement

Figure 15 displays the Vickers microhardness profiles across the weldment region. All three joints have higher microhardness in the FZ than the as-received Cp-Al, which may be attributed to the finer grains in the FZ of the EB welded Cp-Al. The microhardness at the interface of base metal and FZ decreases continuously as we move away from the FZ, which may be attributed to the coarser grains across

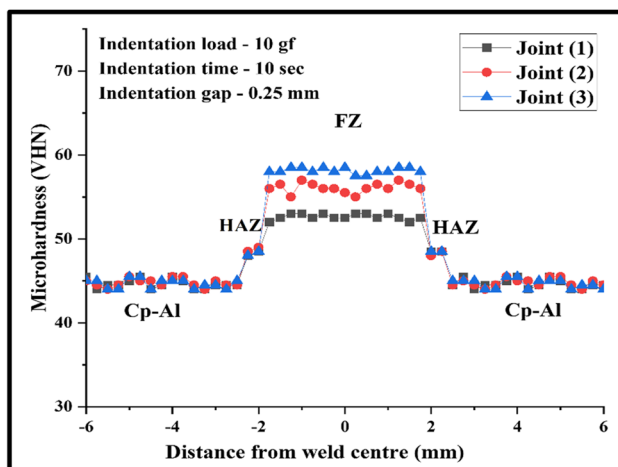


Fig. 15 Variation of microhardness across the weld zone of EB welded Cp-Al joints

the HAZ. The highest average microhardness value of 58 VHN was obtained for joint 3 prepared using a 2-mm oscillation diameter compared to 45 VHN for as-received Cp-Al. The joint prepared with the static beam shows the minimum microhardness of 52 VHN among all the EB welded joints. The introduction of beam oscillations increased the average microhardness (56 VHN—joint 2), which continued to increase with beam oscillation diameter. The increased microhardness due to EB welding was attributed to microstructure refinement, which was even more when BO was used. The hardening mechanism in the weld zone of EB welded Cp-Al was grain refinement following the Hall–Petch equation [29]. Increased microhardness with an increase in beam oscillation diameter is because of the development of finer microstructure. Jeetendra et al. [22] also showed increased microhardness in the weld zone with the oscillated beam.

3.7 Tensile strength and fractography

Figure 16 shows the engineering stress–strain diagram of as-received Cp-Al and EB welded Cp-Al joints prepared using a static beam and oscillated beam having oscillation diameters of 1 mm and 2 mm. Table 3 summarises the parameters derived from tensile testing regarding YS, UTS and percentage elongation of as-received and EB welded Cp-Al. From Table 3, it may be noted that EB welding with a static beam leads to a slight reduction in YS (65 to 62 MPa), UTS (102 to 99 MPa) and percentage elongation (23 to 9%) as compared to as-received Cp-Al. Beam oscillation leads to a further reduction in YS and UTS, but there is a significant improvement in percentage elongation. The increased oscillation diameter does not lead to any significant improvement in YS (47 MPa and 55 MPa) and UTS (91 MPa and

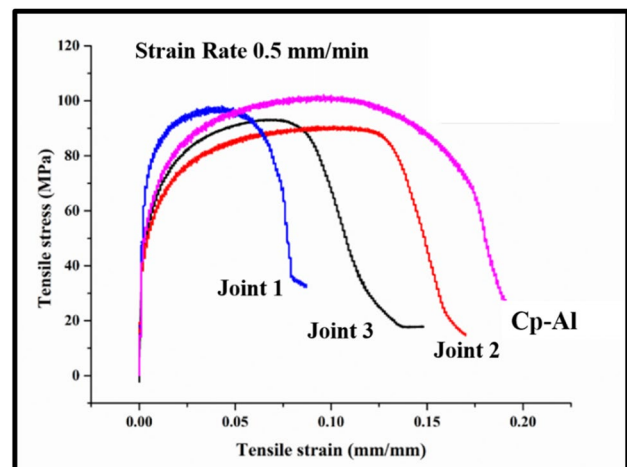


Fig. 16 Engineering stress–strain diagram of as-received and EB welded Cp-Al joints

Table 3 Tensile tests result of the as-received and EB butt welded Cp-Al joints

Specimen designation	YS (MPa)	UTS (MPa)	Percentage elongation (%)	Failure location
As-received Cp-Al	65 ± 2	102 ± 2	23	
Joint-1	62 ± 3	99 ± 2	9	Weld
Joint-2	47 ± 2	91 ± 3	17	Weld
Joint-3	55 ± 1	93 ± 2	15	Weld

93 MPa); rather, percentage elongation (17 to 15%) is marginally reduced. Dinda et al. [25] reported the influence of beam oscillation on EB welding of DP600 steel to Al5754 alloy and concluded that the optimum diameter value needs to be chosen for the best weld properties. Hence, from the present investigation, it may be concluded that 1-mm beam oscillation diameter is the optimum oscillation diameter, which results in the maximum improvement in percentage elongation. The improvement in percentage elongation in case of oscillated beam joints may be corroborated with isotropic equiaxed structure in oscillated beam joints as compared to anisotropic columnar structure in static beam joints. The isotropic equiaxed structure prohibits the spread of cracks in the fusion zone, which helps in increasing the percentage of elongation.

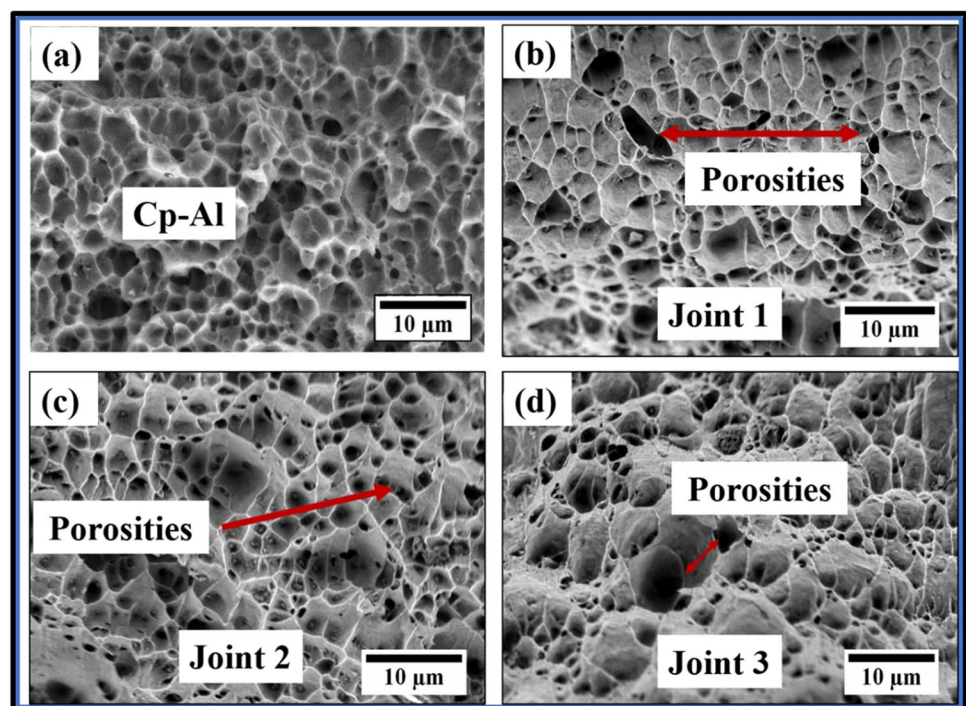
Figure 17a–d shows the fractographs of the fractured surface of (a) as-received Cp-Al, EB welded Cp-Al joints prepared using (b) static beam, oscillated beam having oscillation diameter of (c) 1 mm and (d) 2 mm. From Fig. 17a, it may be noted that failure in Cp-Al is predominantly ductile, evident from dimples. On the other hand, the EB welded

samples have porosities and microcracks. A close comparison of Fig. 17b–d shows that tiny pores and coalescences of micro-voids lead to microcrack formation. The porosities and microcracks are possible sites for crack initiation, as a result of which joint 1 shows minimum ductility. Figure 17c and Fig. 17d show that there is the presence of very small porosities, and the size of dimples is non-uniform. The area fraction of pores is higher in Fig. 17b–d than in Fig. 17a, as a result of which EB welded Cp-Al shows lower ductility than the as-received one. A comparison between joints 2 and 3 further reveals that joint 2 shows relatively higher ductility than joint 3 (cf. Table 3). This is also evident from the fractography of Fig. 17c, which shows the presence of a lower area fraction of porosities compared to Fig. 17b and Fig. 17d in addition to a reduced size.

3.8 Corrosion studies

The corrosion resistance properties of the as-received and the weld zone of EB welded Cp-Al samples were evaluated in a 3.56 wt% NaCl solution by potentiodynamic

Fig. 17 Fractographic images of **a** as-received Cp-Al and EB welded Cp-Al joints prepared using **b** static beam and oscillated beam having oscillation diameter of **c** 1 mm and **d** 2 mm



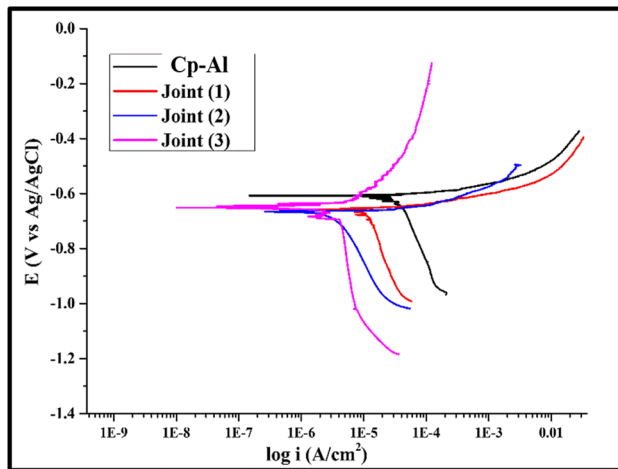


Fig. 18 Potentiodynamic polarisation curves for the as-received, and EB welded Cp-Al joints in 3.5 wt% NaCl solution, showing the variation of current density with applied voltage

Table 4 Results of corrosion test derived from the potentiodynamic polarisation plot

Sample ID	E_{corr} (mV (SCE))	I_{corr} (A)	Corrosion rate (mm/year)
As-received Cp-Al	-606.36	1.88×10^{-6}	0.020351
Joint (1)	-659.11	3.51×10^{-6}	0.037954
Joint (2)	-656.73	3.63×10^{-7}	0.003576
Joint (3)	-649.78	1.07×10^{-7}	0.001271

polarisation test. Figure 18 shows the potentiodynamic polarisation curves of as-received and EB welded Cp-Al in terms of variation of $\log(i)$ as a function of applied potential. Table 4 summarises the corrosion test results derived from the potentiodynamic polarisation plot in terms of corrosion potential (E_{corr}), corrosion current (I_{corr}) and corrosion rate derived from Tafel's extrapolation. From Fig. 18 and Table 4, it may be noted that there is a marginal shift in E_{corr} values in EB welded Cp-Al towards the active direction (-649.8 mV (SCE) to -659.1 mV (SCE)) as compared to -606.4 mV (SCE) of as-received Cp-Al. This marginal shifting in E_{corr} towards an active direction is possibly attributed to the refinement of microstructure, which makes the weld zone more reactive. Though the corrosion potential of EB welded Cp-Al is more active than as-received Cp-Al. However, there is a significant reduction in corrosion rate in the weld zone compared to as-received samples. Furthermore, the joint prepared with a 2-mm beam oscillation diameter shows the minimum corrosion rate (0.001271 mm/year). During EB welding, the fast melting and cooling of the metal produce a fine-grained homogenised microstructure on the surface, which increases the corrosion resistance

of the oscillated weld joints because of the formation of the stronger passive layer, which was also reported earlier [30, 31].

4 Summary and conclusion

In the present study, EB welding of Cp-Al was carried out using varying beam oscillation diameters. From the detailed study, the following conclusions may be drawn:

1. Average surface roughness increased after EB welding and was even higher when beam oscillation was employed than the static beam. The surface roughness increases with an increase in oscillation diameter.
2. Porosities were present predominately at the weld zone and base metal interface. When the static beam was used, the porosity distribution across the weld zone was not uniform. The introduction of beam oscillation reduced the porosity formation (0.02% for the static beam to 0.01% for the oscillated beam) and made the porosity distribution uniform.
3. Due to beam oscillation, an increased area fraction of equiaxed grains is formed in contrast to columnar morphology obtained using a static beam. There is significant refining of microstructure due to EB welding, and refinement was even greater when BO was employed.
4. The microhardness of the EB welded joints (52 VHN to 58 VHN) was higher as compared to the as-received Cp-Al (45 VHN). The introduction of beam oscillation and increased oscillation diameter further increased the microhardness. The highest microhardness of 58 VHN was found for joint 3, prepared with a 2-mm beam oscillation diameter.
5. The YS (62–47 MPa), UTS (99–91 MPa) and % elongation (17–9%) decreased after EB welding as compared to as-received Cp-Al (65 MPa, 102 MPa, and 23%). The joint prepared with the static beam showed the maximum YS (62) and UTS (99 MPa) and minimum % elongation (9%) among the EB welded samples. The introduction of beam oscillation reduced the YS and UTS further but increased the % elongation. The YS, UTS and % elongation did not show any trend with the increase in oscillation diameter. The joint prepared with a 1-mm beam oscillation diameter showed maximum ductility (17%).
6. The corrosion resistance of EB welded samples with the static beam is decreased (corrosion rate, 0.037 mm/year) compared to as-received Cp-Al (0.020 mm/year). However, welding with beam oscillation decreases the corrosion rate (0.003 to 0.001 mm/year) and increases the corrosion resistance. Joint 3, prepared with a 2-mm oscillation diameter, showed a minimum corrosion rate.

Acknowledgements The authors would like to express appreciation for the support of the technical staff of IIT Kharagpur in preparing the electron beam welded Cp-Al samples as well as in characterisation. Partial financial support from Alexander von Humboldt Foundation (Friedrich Wilhelm Bessel Award Scheme to JDM) is also gratefully acknowledged.

Funding The partial financial support from the Board of Research in Nuclear Science (BRNS) (to JDM) and the Ministry of Human Resource Development (to AR) is gratefully acknowledged. Partial financial support from Alexander von Humboldt Foundation (to JDM) is also gratefully acknowledged.

Data Availability All the data related to the manuscript is there in the form of graph or table. Any other data will be made available upon request.

Declarations

Competing interests The authors declare no competing interests.

References

- Dursun T, Soutis C (2014) Recent developments in advanced aircraft aluminium alloys. *Mater Des* 56:862–871. <https://doi.org/10.1016/j.matdes.2013.12.002>
- Miller WS, Zhuang L, Bottema J et al (2000) Recent development in aluminium alloys for the automotive industry. *Mater Sci Eng A* 280:37–49. [https://doi.org/10.1016/S0921-5093\(99\)00653-X](https://doi.org/10.1016/S0921-5093(99)00653-X)
- Cole GS, Sherman AM (1995) Light weight materials for automotive applications. *Mater Charact* 35:3–9. [https://doi.org/10.1016/1044-5803\(95\)00063-1](https://doi.org/10.1016/1044-5803(95)00063-1)
- Zhu Q, Yu H, Zhang J, et al (2021) Experimental study on tig welding properties of 6061 and 7003 aluminum alloys. *IOP Conf Ser Earth Environ Sci* 621. <https://doi.org/10.1088/1755-1315/621/1/012060>
- Schubert E, Klassen M, Zerner I et al (2001) Light-weight structures produced by laser beam joining for future applications in automobile and aerospace industry. *J Mater Process Technol* 115:2–8. [https://doi.org/10.1016/S0924-0136\(01\)00756-7](https://doi.org/10.1016/S0924-0136(01)00756-7)
- Löveborn D, Larsson JK, Persson KA (2017) Weldability of aluminium alloys for automotive applications. *Phys Procedia* 89:89–99. <https://doi.org/10.1016/j.phpro.2017.08.011>
- Lee SJ, Nakamura H, Kawahito Y, Katayama S (2014) Effect of welding speed on microstructural and mechanical properties of laser lap weld joints in dissimilar Al and Cu sheets. *Sci Technol Weld Join* 19:111–118. <https://doi.org/10.1179/1362171813Y.0000000168>
- Alali M, Todd I, Wynne BP (2017) Through-thickness microstructure and mechanical properties of electron beam welded 20 mm thick AISI 316L austenitic stainless steel. *Mater Des* 130:488–500. <https://doi.org/10.1016/j.matdes.2017.05.080>
- Vänskä MP, Kujanpää V, Westin EM, Torvinen T (2009) Short focal length scanner fiber laser welding of stainless steel sheets and tubular products. *ICALEO 2009–28th Int Congr Appl Lasers Electro-Optics*. Congr Proc 102:766–772. <https://doi.org/10.2351/1.5061641>
- Wang L, Liu Y, Yang C, Gao M (2021) Study of porosity suppression in oscillating laser-MIG hybrid welding of AA6082 aluminum alloy. *J Mater Process Technol* 292:117053. <https://doi.org/10.1016/j.jmatprotec.2021.117053>
- Meng Y, Yu Q, Gao M et al (2024) High-frequency oscillating laser-arc hybrid welding of 8-mm-thick high-strength aluminum alloy through synchronous wire-powder feeding. *Int J Heat Mass Transf* 222:125180. <https://doi.org/10.1016/j.ijheatmasstransfer.2024.125180>
- Wang L, Gao M, Zhang C, Zeng X (2016) Effect of beam oscillating pattern on weld characterization of laser welding of AA6061-T6 aluminum alloy. *Mater Des* 108:707–717. <https://doi.org/10.1016/j.matdes.2016.07.053>
- Berend O, Haferkamp H, Meier O, Engelbrecht L (2005) High-frequency beam oscillating to increase the process stability during laser welding with high melt pool dynamics. *24th Int Congr Appl Lasers Electro-Optics, ICALEO 2005 - Congr Proc* 2206:1032–1041. <https://doi.org/10.2351/1.5060476>
- Jha MN, Pratihari DK, Dey V et al (2011) Study on electron beam butt welding of austenitic stainless steel 304 plates and its input-output modelling using neural networks. *Proc Inst Mech Eng Part B J Eng Manuf* 225:2051–2070. <https://doi.org/10.1177/0954405411404856>
- Lipińska M, Pixner F, Szachogluchowicz I et al (2023) Application of electron beam welding technique for joining coarse-grained and ultrafine-grained plates from Al-Mg-Si alloy. *J Manuf Process* 104:28–43. <https://doi.org/10.1016/j.jmapro.2023.08.057>
- Babu NK, Raman SGS, Murthy CVS, Reddy GM (2005) Influence of beam oscillation patterns on the structure and mechanical properties of Ti-6Al-4V electron beam weldments. *Sci Technol Weld Join* 10:583–590. <https://doi.org/10.1179/174329305X57473>
- Barbieri G, Moncada M, Sgambati A (2012) EBW of AA 6061 T651 aluminium alloy cold plates for the space guinea pig living unit cooling system. *Weld Int* 26:360–369. <https://doi.org/10.1080/09507116.2011.592693>
- Elseddig Z, Sobih M, Almazy K, Sallam M (2010) Experimental investigation of electron beam welding of AA1350 aluminum alloy. *Int Conf Appl Mech Mech Eng* 14:1–11. <https://doi.org/10.21608/amme.2010.37523>
- Moschinger M, Mittermayr F, Enzinger N (2022) Influence of beam figure on porosity of electron beam welded thin-walled aluminum plates. *Materials (Basel)* 15:1–14. <https://doi.org/10.3390/ma15103519>
- Zhan X, Yu H, Feng X, et al (2019) A comparative study on laser beam and electron beam welding of 5A06 aluminum alloy. *Mater Res Express* 6. <https://doi.org/10.1088/2053-1591/ab0562>
- Kar J (2023) Effect of process parameters on porosities in electron beam welded AA-6061 to AA-2024 dissimilar joints. *Weld World* 67:2007–2016. <https://doi.org/10.1007/s40194-023-01549-9>
- Singh JK, Roy GG, Majumdar JD (2022) Effect of beam oscillation on microstructure and tensile property of electron beam-welded commercially pure (CP) titanium. *Trans Indian Inst Met.* <https://doi.org/10.1007/s12666-022-02793-1>
- Nair BS, Phanikumar G, Prasad Rao K, Sinha PP (2007) Improvement of mechanical properties of gas tungsten arc and electron beam welded AA2219 (Al-6 wt-%Cu) alloy. *Sci Technol Weld Join* 12:579–585. <https://doi.org/10.1179/174329307X227210>
- Mastanaiah P, Sharma A, Reddy GM (2018) Process parameters-weld bead geometry interactions and their influence on mechanical properties: a case of dissimilar aluminium alloy electron beam welds. *Def Technol* 14:137–150. <https://doi.org/10.1016/j.dt.2018.01.003>
- Dinda SK, Kar J, Jana S et al (2019) Effect of beam oscillation on porosity and intermetallics of electron beam welded DP600-steel to Al 5754-alloy. *J Mater Process Technol* 265:191–200. <https://doi.org/10.1016/j.jmatprotec.2018.10.026>
- Pham MS, Dovgvy B, Hooper PA et al (2020) The role of side-branching in microstructure development in laser powder-bed fusion. *Nat Commun* 11:1–12. <https://doi.org/10.1038/s41467-020-14453-3>

27. Cao X, Wallace W, Immarigeon JP, Poon C (2003) Research and progress in laser welding of wrought aluminum alloys. II. Metallurgical microstructures, defects, and mechanical properties. *Mater Manuf Process* 18:23–49. <https://doi.org/10.1081/AMP-120017587>
28. Singh JK, Roy GG, Majumdar JD (2023) Studies on the effect of process parameter on corrosion behaviour of electron beam welded Ti-based alloy (Ti6Al4V). *Weld World* 67:2731–2747. <https://doi.org/10.1007/s40194-023-01599-z>
29. Alshabat N, Al-qawabah S (2015) Effect of 4%wt. Cu addition on the mechanical characteristics and fatigue life of commercially pure aluminum. *Jordan J Mech Ind Eng* 9:297–301
30. Ma S, Zhao Y, Zou J et al (2017) The effect of laser surface melting on microstructure and corrosion behavior of friction stir welded aluminum alloy 2219. *Opt Laser Technol* 96:299–306. <https://doi.org/10.1016/j.optlastec.2017.05.028>
31. Osório WR, Freire CM, Garcia A (2005) The role of macrostructural morphology and grain size on the corrosion resistance of Zn and Al castings. *Mater Sci Eng A* 402:22–32. <https://doi.org/10.1016/j.msea.2005.02.094>

Publisher's Note Springer Nature remains neutral with regard to jurisdictional claims in published maps and institutional affiliations.

Springer Nature or its licensor (e.g. a society or other partner) holds exclusive rights to this article under a publishing agreement with the author(s) or other rightsholder(s); author self-archiving of the accepted manuscript version of this article is solely governed by the terms of such publishing agreement and applicable law.